Valence Charge Concentrations, Electron Delocalization and β-Agostic Bonding in d^0 Metal Alkyl Complexes

Wolfgang Scherer,*[a] Peter Sirsch,[a] Dmitry Shorokhov,[a] Maxim Tafipolsky,[a] G. Sean McGrady,*[b] and Emanuel Gullo[c]

Abstract: In this paper we describe a range of model d^0 metal ethyl compounds and related complexes, studied by DFT calculations and high resolution X-ray diffraction. The concept of ligand-opposed charge concentrations (LOCCs) for d^0 metal complexes is extended to include both *cis*-and *trans*-ligand-induced charge concentrations (LICCs) at the metal, which arise as a natural consequence of covalent metal–ligand bond formation in transition metal alkyl complexes. The interplay between *locally* induced sites of increased Lewis acidity and an ethyl ligand is crucial to the development of a β-agostic interaction in d^0 metal alkyl complexes, which is driven by delocalization of the M–C bonding electrons. Topological analysis of theoretical and experimental charge densities reveals LICCs at the metal atom, and indicates delocalization of the M–C valence electrons over the alkyl fragment, with depletion of the metal-directed charge concentration (CC) at the α-carbon atom, and a characteristic ellipticity profile for the C_α–C_β bond. These ellipticity profiles and the magnitude of the CC values at C_α and C_β provide experimentally observable criteria for assessing quantitatively the extent of delocalization, with excellent agreement between experiment and theory. Finally, a concept is proposed which promises systematic control of the extent of C–H activation in agostic complexes.

Keywords: agostic interactions · charge concentrations · charge density analysis · delocalization · transition metals

Introduction

Transition metal alkyl complexes with a d^0 electron configuration commonly exhibit structures which confound expectations based on simple models such as the VSEPR theory.[1] These fall into two apparently distinct classes,[2] namely i) systems such as WMe_6[3] or Me_2TiCl_2,[4] in which the metal–alkyl geometry appears more-or-less normal but the skeletal geometry deviates from VSEPR predictions; and ii) complexes such as $[RTiCl_3(dmpe)]$ (R = Me, Et; dmpe = $Me_2PCH_2CH_2PMe_2$),[5] in which the whole metal–alkyl moiety is severely distorted, leading to an agostic structure displaying close M···H–C contacts.[6]

On the basis of combined experimental and theoretical studies of $[EtTiCl_3(dmpe)]$ and related complexes, we have recently proposed a bonding model for β-agostic interactions in early transition metal complexes which considers the interaction to derive primarily from delocalization of the M–C_α bonding electrons, rather than from any significant M···H–C_β interaction.[7a–d] In another recent contribution, we demonstrated that this type of electron delocalization in organolithium compounds can be described in terms of the well-known phenomenon of negative hyperconjugation, assisted by additional secondary interactions between the Lewis acidic metal and the alkyl fragment.[7e,f]

The energetic stabilization which attends resonance or electron delocalization[8] is a central feature of both the valence bond[9] and the molecular orbital[10] approaches to bonding. Whilst it represents an elegant concept, hyperconjugative delocalization is very difficult to represent quantitatively on the basis of experimental observables. Thus, whereas its geometrical consequences can be followed by

[a] Prof. Dr. W. Scherer, P. Sirsch, Dr. D. Shorokhov, Dr. M. Tafipolsky
Institut für Physik, Universität Augsburg
Universitätsstrasse 1, 86159 Augsburg (Germany)
Fax: (+49)-821-598-3227
E-mail: wolfgang.scherer@physik.uni-augsburg.de

[b] Dr. G. S. McGrady
Department of Chemistry, University of New Brunswick
Fredericton, N. B., E3B 6E2 (Canada)
E-mail: smcgrady@unb.ca

[c] E. Gullo
Department of Chemistry, King's College London
Strand, WC2R 2LS (UK)

Supporting information for this article is available on the WWW under http://www.chemeurj.org or from the author; it includes: listings of geometrical and topological parameters, fractional atomic coordinates and mean square atomic displacement parameters, multipole population coefficients, expansion-contraction coefficients, descriptions of the local coordinate sytems used in the multipole refinements, and residual electron density maps for $[EtTiCl_3(dmpe)]$ **5** and Bz_3Ti-O-$TiBz_3$; basis set description for Ti.

 DOI: 10.1002/chem.200304909

careful structural studies, concomitant changes in the electronic structure are rather difficult to trace by experiment. However, analysis of the topology of the charge density exploiting the "atoms-in-molecules" (AIM) approach[11] offers a powerful method with which to analyze the electronic effects of delocalization. Bader et al. and Cremer et al. have related conjugative interactions to the existence of ellipticity of the electron distribution (ε) in a bond, thus establishing a direct link with the (observable) molecular charge density.[12a,b] According to these studies, hyperconjugation is also revealed by the bond order n, which can be evaluated in terms of the charge density at the bond critical point (BCP), $\rho(\boldsymbol{r}_c)$.[12b] Accordingly, C–C bonds with $n > 1$ and $\varepsilon > 0$ can show evidence of hyperconjugative interactions. However, experimental evidence for charge transfer from a carbanion lone pair to an electronegative group, or of charge delocalization due to negative hyperconjugation, remains elusive. In order to observe such effects experimentally, charge-density based criteria such as analysis of atomic charges,[11] valence shell charge concentrations[13] and atomic dipole or quadrupole polarizations[12c, 14] must be employed.

In this paper, we apply theoretical and experimental methods to analyze the topology of the charge density distribution in a series of d^0 metal ethyl complexes and related species. We demonstrate that the charge concentrations in the valence shell of the α- and β-carbon atoms of the ethyl fragment vary with the extent of delocalization of the M–C bonding electrons over the alkyl fragment, and we show that the alkyl ligand induces charge concentrations at a d^0-metal center that are responsible for *both* types of structural deformation described above. We also propose the concept of bond path ellipticity as novel and general measure of the nature and extent of delocalization in an agostic system. Finally, a concept is introduced which holds out the prospect of manipulating the extent of C–H activation in potential agostic systems by controlling and modeling the ligand-induced charge polarization of the transition metal atom.

Results and Discussion

Non-VSEPR geometries of d^0 metal complexes: In an elegant study by Gillespie et al.,[15] the monomeric alkaline-earth dihalides were examined using the AIM method of Bader.[11] The heavier congeners (Ca–Ba) are remarkable in displaying bent rather than linear geometries as are observed for the dihalides of Be and Mg. These unusual bent geometries, initially established by experiment,[16, 17] have been the subject of several theoretical studies.[3f, 17c,d, 18] Apart from BaF_2, the barrier to linearity is no greater than 2 kcal mol^{-1}; hence these systems are more realistically described as quasilinear. Whilst neither a simple ionic model nor the VSEPR concept[1] can account for these distortions, the more sophisticated polarized ion model[19a–c] predicts the correct geometries of the individual alkaline earth dihalides. Thus, the polarizability of the metal seems to be a primary factor in promoting nonlinearity. However, Schleyer et al. observed systematic differences between the bending force constants obtained by the polarized ion model and by ab initio methods:[18b] participation of d orbitals on the metal atom decreases the force constants for the heavier dihalides (Ca – Ba). Thus, the atomic d orbitals should be relatively unimportant for Be and Mg but should increase in importance in going from Ca to Ba, as noted earlier by Hayes.[19d] Hence, both polarization of the metal (an ionic effect) and d orbital participation (a covalent contribution) affect the bending potential in these molecules. As noted by Szentpály and Schwerdtfeger, these factors are not different; rather are they two sides of the same coin, since it is the subvalence $(n-1)$d orbitals that are responsible for the polarization of the metal cores.[20]

As an alternative to the polarized ion model, which describes these distortions mainly in terms of electrostatic interactions, Gillespie et al. proposed topological analysis of the charge density as a non-empirical way of accounting for the polarization, and discovered so-called ligand-opposed charge concentrations (LOCCs) to exist *trans* to the M–X bonds in the nonlinear alkaline-earth dihalides.[15] In fact, Bader et al. had shown in an earlier study that the presence of ligands in covalent or polar molecules induces local charge concentrations (CCs) in the valence shell of atoms which are revealed by AIM analysis as $(3,-3)$ critical points (CPs) in the negative Laplacian $L(\boldsymbol{r}) = -\nabla^2\rho(\boldsymbol{r})$ of the charge density.[21] Furthermore, the number and relative positions of these charge concentrations have been shown to recover the number and relative positions of the localized electron pairs (electron pair domains) associated with the bonding and nonbonding electron pairs of the VSEPR model, thereby endowing it with a sound physical basis.[21a]

The non-VSEPR geometries observed for the heavier alkaline earth and d^0 transition metal systems arise naturally when LOCCs are brought into the picture. Now, not just the bonding electron pair domains, but also the LOCCs each make spatial demands at the central atom, the global solution of which leads to the lowest energy configuration. The more covalent the M–L bond, the greater the LOCC which it induces, accounting for the proclivity of alkyl ligands to shy away from a mutually *trans* disposition in d^0 complexes.[3, 22]

In the following two Sections, we explore the concept and nature of CCs in d^0 transition metal alkyl complexes, we highlight potential confusion in the terminology relating to VSCCs, and we identify for the first time the origin and nature of LOCCs.

Charge concentrations in $[MeCa]^+$ (1): With only a few exceptions, the successes of the strikingly simple VSEPR model are confined to the lighter main group elements. The situation becomes more complicated when the polarization of transition metals or of the heavier alkaline earth elements (Ca, Sr, Ba) is analyzed. We illustrate this point by reference to the simple cationic alkyl systems $[MeCa]^+$ (**1**) and $[EtCa]^+$ (**2**) (Figure 1). According to Bader et al. the Laplacian recovers the shell structure of atoms,[23] since the radii at which $L(\boldsymbol{r})$ attains a maximum value define spheres upon which electronic charge is concentrated. For elements with $Z \leq 18$, one sphere is observed for each quantum shell. The radii of these spheres of charge concentration are characteristic for each shell of each atom, and thus provide an unambiguous identification of the corresponding quantum shell.[11, 23] How-

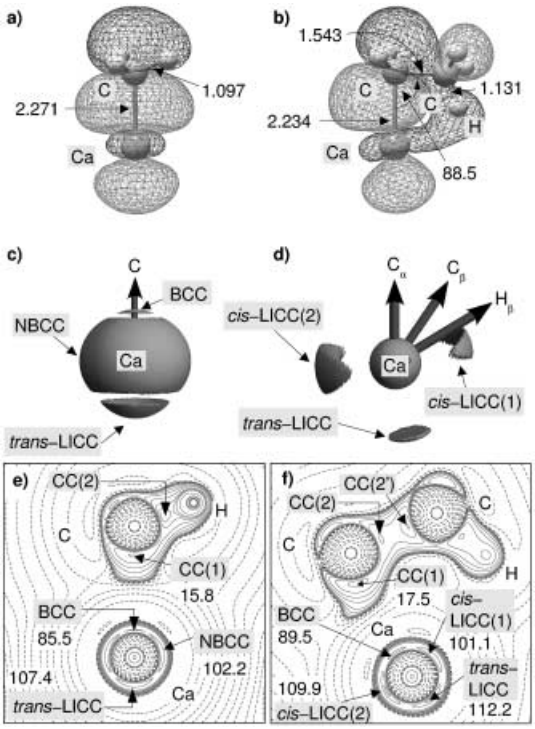

Figure 1. a), b): Constant probability density surface for the HOMO of $[MeCa]^+$ (**1**) and $[EtCa]^+$ (**2**), respectively. Distances in [Å] and bond angles in [°]. c), d): Isovalue surface (envelope) plots of the negative Laplacian [$L(\boldsymbol{r}) = 84$ and 101 e Å^{-5}, respectively] for the Ca center in **1** and **2**. e), f): Contour plot of the negative Laplacian of the charge density, $L(\boldsymbol{r})$, in the Ca-C-H plane of **1**, and the Ca-C-C plane of **2**, respectively. Default contour levels are drawn at $+0.001$, $\pm 2.0 \times 10^n$, $\pm 4.0 \times 10^n$, $\pm 8.0 \times 10^n$ e Å^{-5}, where $n = 0$, ± 3, ± 2, ± 1; positive and negative values are marked by solid and dashed lines, respectively. Extra contour lines at 15, 25, 84, 105, 240, 280, 350 e Å^{-5} are drawn and the contour lines at 80, 200 and 400 were skipped to reveal the relative positions of the CCs. This will be our default setting in the following. The relative locations of the bonding charge concentration BCC, of the ligand induced charge concentration LICC and of the diffuse feature representing the nonbonding charge concentration NBCC in **1** are indicated by arrows. In **2**, the diffuse feature, labeled NBCC, has been polarized by the agostic ethyl ligand, resulting in two *cis*-oriented CCs.

ever, as noted by Bader et al., the shell structure for the transargonic elements is not fully represented by the Laplacian. Thus, only three instead of four shells of charge concentration are observed for the calcium atom, [Ar]4s^2. The same is true for the calcium atom in **1** and **2**. In general the fourth, fifth or sixth shell for elements of Period 4–6, respectively, is not revealed in the Laplacian.[24]

The $L(\boldsymbol{r})$ contour maps of the calcium atom in **1** and **2**, Figures 1e and f clearly reveal the presence of CCs within the outer (third) shell of the core of $L(\boldsymbol{r})$. Thus, it is the charge distribution in the $(n-1)$ quantum shell that is distorted by the presence of ligands, rather than that in the n quantum shell as for a p-block element with $Z \leq 18$.[25] Recent quantum chemical studies have clearly demonstrated the CCs present in the $(n-1)$ outer shell of the core of d-block elements to arise from polarization of the $(n-1)$d and ns valence electrons.[26] Bader et al. concluded that the $(n-1)$ outer shell of the core as defined by $L(\boldsymbol{r})$ is, in effect, the valence shell of a transition metal atom,[26] a conclusion in accord with the ubiquitous participation of the $(n-1)$d orbitals in the chemistry of transition metals. Hence, the distinction between local maxima in the so-called valence shell charge concentration (VSCC) for elements with $Z \leq 18$ and local maxima in the outer shell of charge concentration for transargonic elements is purely a formal one. Both types of local maxima or charge concentrations arise from distortion of the valence electron density. Accordingly, we use the general term CC to discuss polarization or distortion of the electron density, irrespective of the principal quantum shell of the atom at which it occurs.

Charge concentrations in $[EtCa]^+$ (2)–Electron delocalization and β-agostic interaction: Figure 1e and f show contour maps of the negative Laplacian of the charge density for the electrons in the symmetry plane of $[MeCa]^+$ (**1**) and the Ca-C-C plane in $[EtCa]^+$ (**2**) at the B3LYP/I level of theory (see Experimental Section for a basis set definition; unless specified otherwise, this will be our standard level employed in the density functional theory (DFT) calculations). Positive values of $L(\boldsymbol{r})$ indicate that charge is locally concentrated at $\boldsymbol{r}$, whereas negative $L(\boldsymbol{r})$ values are characteristic of regions suffering local charge depletion. Accordingly, the principal quantum shells of the carbon atoms in **1** and **2**, K and L, are characterized by regions of charge concentration and depletion (Figure 1 e and f). The charge concentration in the L shell of the carbon atoms appears to be rather distorted, showing local maxima and minima. Indeed, $L(\boldsymbol{r})$ in Figure 1e and f reveals two maxima in the L shell of each carbon atom in **1** (Ca-C_α-H plane) and **2** (Ca-C_α-C_β plane). These two maxima, or (3, –3) critical points,[11] are henceforth denoted bonding charge concentrations [bonding CC(1) and CC(2)], since they are located on the Ca–C, C–H or C–C bond paths.[27] In Figure 1e and f the relative positions of CC(1) and CC(2) are revealed by the contour line at 5 e Å^{-5}. In total, four such maxima are evident, located along each of the three or two C–H bonds in **1** and **2**, respectively, the unique C–C bond (in **2**) and the Ca–C bond. In addition to their location, these four CCs can also be classified by their relative magnitudes. Thus, CC(1) for **2**, with a value of 17.5 e Å^{-5}, represents our benchmark value for a "carbanionic" CC directed toward the metal atom. We now demonstrate that the CCs at the calcium atom in $[MeCa]^+$ and $[EtCa]^+$ can also be assigned in a systematic manner and shown to be ligand induced. The first type of charge concentration is assigned straightforwardly: BCC describes the bonding charge concentrations facing the C_α atom of the alkyl groups (Figure 1e and f). This arrangement of facing charge concentrations is typically observed in the case of covalent bonds. Here, the CCs of the two bonding partners of similar electronegativity merge with each other to give a single region of bonding charge concentration, with the characteristic two maxima or (3, –3) CPs.[28] In the case of the Ca–C bond, a low $\rho(\boldsymbol{r})$ value of 0.52 e Å^{-3} in combination with a negative $L(\boldsymbol{r})$ value of –3.6 e Å^{-5} at the Ca–C bond CP of **2** imply pronounced bond polarity. However, energetic considerations and a detailed topological analysis of the charge density at the Ca–C bond CP also support some covalent character.[29]

In addition, analysis of the wavefunction reveals the Ca–C bond to be remarkably covalent and, as for the heavier alkaline earth dihalides,[17d] to have metal d-orbital character. The HOMOs of **1** and **2** are essentially Ca–C σ-bond orbitals formed mainly by combination of the Ca d_{z^2} and the C p_z atomic orbitals (Figure 1a and b). As with the early transition metal systems Me_nTiCl_{4-n} ($n = 1-4$),[30] the M – C bond in both **1** and **2** may be described in terms of sd, rather than sp, hybridization at the metal according to our natural localized molecular orbital (NLMO) analysis.[31] In this respect, **1** and **2** serve as the simplest model systems for d^0 transition metal methyl and ethyl complexes.

The second type of charge concentration in $[MeCa]^+$ (**1**), *trans* to the Ca–C bond, is much more pronounced than the BCC [$L(\boldsymbol{r}) = 107.4$ vs 85.5 e Å^{-5}; Figure 1e], and appears to be ligand induced. This corresponds to the ligand-opposed CCs (LOCCs) postulated by Gillespie et al. for the heavier alkaline earth dihalide molecules.[15] For the reasons explained below we use the term *trans*-ligand-induced CC (*trans*-LICC) to describe this feature. A third type of CC is also apparent in Figure 1c and e; denoted nonbonding charge concentration (NBCC), it is rather diffuse and shows near-perfect cylindrical symmetry.[32] Thus, a significant degree of metal polarization is apparent in **1**, but only a *single* ligand is present.

In the case of the higher homologue $[EtCa]^+$ (**2**), the BCC and *trans*-LICC each appear again. However, in comparison with **1**, these two CCs are more pronounced: $L(\boldsymbol{r}) = 89.5$ e Å^{-5} (BCC) and 112.2 e Å^{-5} (*trans*-LICC). Furthermore, two pronounced CCs are observed orthogonal to the (BCC)-(*trans*-LICC) vector, which we denote *cis*-LICCs. Only *trans*-LICCs (or LOCCs) have been reported hitherto in the literature.[15] As far as we are aware, this is the first report of charge concentrations induced *cis* to a M–C bond. A further difference between **1** and **2** is the overall geometry of the metal – alkyl fragment: the β-CH_3 unit of the ethyl ligand has been canted toward the Ca atom so as to bring a C_β–H_β fragment close to the metal (Ca ··· C_β 2.682, Ca ··· H_β 2.331 Å). In other words, a β-agostic interaction has been established.[33] This has further consequences for the polarization of the metal atom: Figures 1d, and f reveal a pronounced asymmetry in the *cis*-LICCs described above. The proximal C_β–H_β fragment appears to cause a depletion in the magnitude of *cis*-LICC(1) compared with *cis*-LICC(2) [$L(\boldsymbol{r}) = 101.1$ e Å^{-5} vs 109.9 e Å^{-5}].[34]

Hence, for the first time a clear relationship emerges between the charge-density and wavefunction based models of metal atom polarization. In the case of $[MeCa]^+$ (**1**), the HOMO is derived mainly from combination of the d_{z^2} metal orbital and the p_z orbital on the C_α atom of the methyl ligand. Since this is the only bonding interaction between the metal and the solitary ligand, the LICCs *must* be related to the density contours of this MO. The predominance of the d_{z^2} orbital in the metal-based bonding results in a charge distribution which mimics the shape and symmetry of the contours of the d_{z^2} function: two pronounced CCs along the molecular *z* axis and a diffuse belt in the equatorial (*xy*) plane. The β-agostic interaction in $[EtCa]^+$ (**2**) polarizes this belt of CC into the two distinct *cis*-LICCs seen in **2**. Depletion of *cis*-LICC(1) can now be related to the agostic bonding interaction which develops between the metal atom and the β-CH fragment, resulting in a cyclic delocalization of the metal – ligand bonding electrons, as described in our previous analysis of β-agostic interactions in early transition metal alkyl complexes.[7a–d] The HOMO of **2** thus accommodates the total η^2-metal–ethyl bonding interaction within a *single* orbital.[35]

In common with the lithium complex $[2\text{-}(Me_3Si)_2\text{-}CLiC_5H_4N]_2$ (**3**), which displays pronounced negative hyperconjugation, the carbanion charge concentration in the β-agostic system **2** is reduced relative to that in EtLi (**4**) [CC(1) = 17.5 vs 18.9 e Å^{-5}].[7e,f] In common with EtLi,[7e,f] we note a pronounced asymmetry along the C_α–C_β bond in **2** [CC(2) = 15.5/16.3 and CC(2′) = 20.2/20.4 e Å^{-5} in **2** and **4**, respectively (Figure 1f)].

Experimental observation of ligand-induced charge concentrations: In this Section we demonstrate that the polarization pattern induced by an agostic ethyl group in our model system **2** is characteristic of more realistic and complex β-agostic systems. The textbook example in this regard is [Et-$TiCl_3$(dmpe)], the earliest reported β-agostic ethyl complex, and which has since been the subject of numerous experimental and theoretical investigations.[7a–d] Accordingly, [Et-$TiCl_3$(dmpe)] (**5**) serves as our experimental benchmark system (Figures 2 and 3).

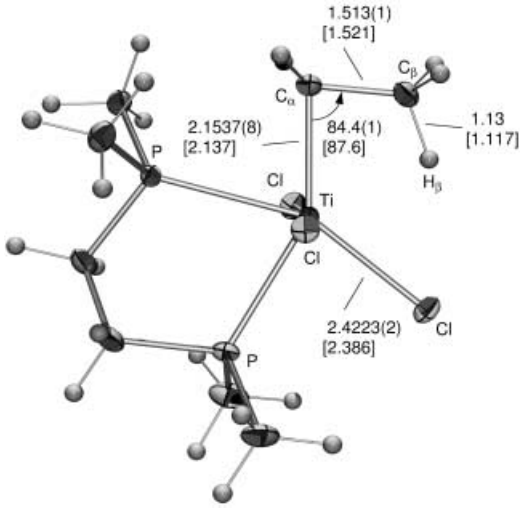

Figure 2. Molecular structure of [$EtTiCl_3$(dmpe)] (**5**) in the solid state at 105 K; 50% probabililty level (after multipolar refinement); salient bond lengths [Å] and angles [°] are specified and compared with the calculated values (in square brackets).

In Figure 3c the $L(\boldsymbol{r})$ plot in the TiCC plane of **5** is shown, after multipolar refinement of all atoms except Ti,[36] which appears completely unpolarized as a consequence. In Figures 3d and e, successive multipoles have been introduced (one hexadecapole with $l = 4$; $m = 0$, and one dipole with $l = 1$; $m = 0$) at the metal center in the refinements (the *z* axis points along the Ti–C_α vector). The main polarization features evident for **2** in Figure 1d and f are thus reproduced satisfactorily for **5**. As a normalized charge density function derived from the spherical harmonics, population of the first multipole (P_{40} hexadecapole) leads to a charge density

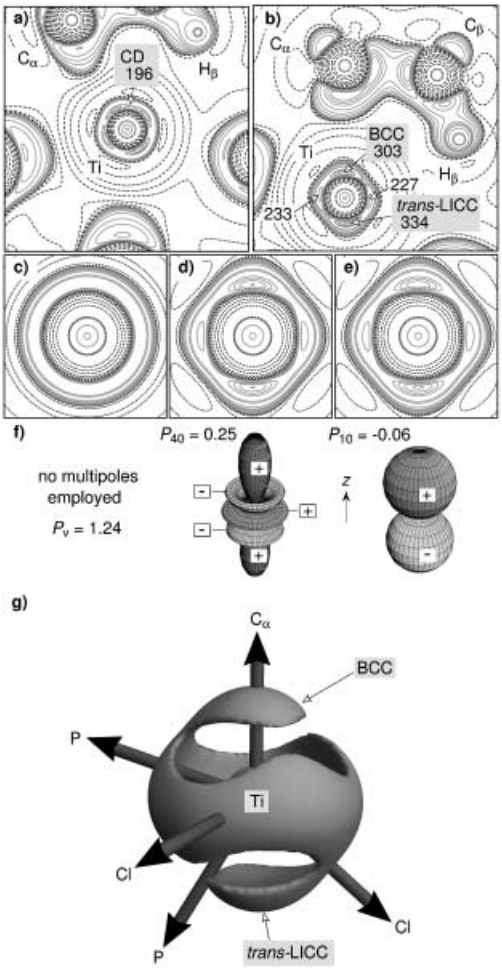

Figure 3. a), b) Contour plot of the negative Laplacian of the theoretical and experimental charge density, $L(\boldsymbol{r})$, in the Ti-C_α-C_β plane of [Et-$TiCl_3$(dmpe)] (**5**), respectively. Flexible multipolar refinement at Ti (hexadecapole level). Besides the extra contour lines at 196 and 320 e Å^{-5} default levels as defined in Figure 1 were used. Only in Figure 3a lines at 20, 25, 84, 105 e Å^{-5} were skipped. c)–e): $L(\boldsymbol{r})$ contour plots in the Ti-C_α-C_β plane of **5** (box size around Ti: 2.5 × 2.5 Å^2; contour levels as above) showing that the distortion of the charge density at the metal can be approximately fitted by just two multipoles: c) Without multipolar refinement of the Ti atom. d) Inclusion of one hexadecapole at Ti ($l = 4$, $m = 0$). e) Inclusion of an additional dipole at Ti ($l = 1$, $m = 0$). f) Representation of the shape of the density-based multipoles (hexadecapole [$l = 4$, $m = 0$] and dipole [$l = 1$, $m = 0$], respectively). g) Experimental envelope map ($L(\boldsymbol{r}) =$ 160 e Å^{-5}) showing the ligand-induced polarization at the Ti atom in **5**.

distribution at the metal which mimics approximately the isovalue density contours of a d_{z^2} orbital.[37] Thus, it mainly accounts for the axial (along the Ti–C vector) and equatorial polarization of the metal atom. Owing to its mathematical definition as a normalized density function, population of this multipole alone results in a BCC and a *trans*-LICC of equal magnitude and a diffuse NBCC feature with cylindrical symmetry (Figure 3d). Accordingly, a second multipole (Ti–C bond-directed dipole) is needed to account for the different magnitudes of the BCC and the *trans*-LICC [303 and 334 e Å^{-5}, respectively] in our final experimental model which is based on a flexible multipolar refinement (Figure 3b, e). As shown by the $L(\boldsymbol{r})$ contour maps in Figure 3a and b, the experimental polarization pattern is in good agreement with our theoretical model.[38]

Hence, a simple multipolar model accounts for the polarization of the metal atom by an agostic ethyl group in **5**, in pleasing agreement with our interpretation of the wavefunction for **2** (previous Section).[39]

These results represent an important advance, for they demonstrate *cis*-LICCs to be observable not just by calculation, but also from analysis of the experimental molecular charge density; and confirm their existence as a real phenomenon which warrants further experimental and theoretical investigation.

Bond ellipticity as a measure of charge delocalization in agostic systems: At this stage, it is appropriate to introduce a novel, charge-density based criterion which accounts for electron delocalization within an alkyl group. Figure 1f reveals the ethyl ligand in **2** to be polarized in such a way that charge is locally concentrated [$L(\boldsymbol{r}) > 0$] on the face directed toward the Lewis-acidic metal center. This contrasts with the non-agostic ethyl ligand in EtLi (**4**), where a pronounced charge depletion is observed at the β-carbon atom facing the Li center.[7f] We have previously shown the transition from non-agostic $EtTiCl_3$ (**6**) to the β-agostic adduct [$EtTiCl_3$(dmpe)] (**5**) to be accompanied by a global bonding redistribution within the Ti-CH_2-CH_3 moiety.[7d] We now demonstrate that this global redistribution is a natural consequence of delocalization of the M–C bonding electrons. This becomes evident when the bond ellipticity is traced along the full C_α–C_β bond path. To illustrate the point, we introduce $[EtTiCl_2]^+$ (**7**) as a model β-agostic system for **5**. $[EtTiCl_2]^+$ preserves the essential electronic features of the metal–ethyl bonding in **5** whilst avoiding complications from steric factors,[40–42] and shows a more pronounced β-agostic interaction than does **5**.[7a,c] These advantages have resulted in its use as a model system for cationic metallocene-based Ziegler–Natta catalysts.[43] We have previously demonstrated the existence of two β-agostic conformers for **7**, with eclipsed (**7a**) or staggered (**7b**) C_β–H_β conformations with respect to the M–C_α bond.[44]

According to the mathematical definition (Figure 4), ε values greater than zero indicate partial π-character in a bond, or electronic distortion away from σ-symmetry along the bond path.[12b] Indeed, the ellipticity profiles of both staggered and eclipsed conformers of $[EtTiCl_2]^+$ (**7**) along the C_α–C_β bond path reveal significant π-character. However, both profiles show a rather complex pattern in comparison with the standard C–C single or double bond in C_2H_6 and C_2H_4, respectively, or in the metallacycle [(η^2-C_2H_4)$TiCl_2$] (**8**) (Figure 4).[12d] Whereas for C_2H_6 ε is zero along the full bond path, C_2H_4 and the metal complex **8** show pronounced ellipticities. C_2H_4 shows a maximum ε value (ε_{max}) of 0.34 at the bond CP. In comparison with C_2H_4, the metallacycle **8** reveals a broader ellipticity profile with a pronounced double maximum ($\varepsilon_{max} = 0.31$).[45] This arises from differences in the π-bonding between C_2H_4 and **8** (see below). For the staggered form of $[EtTiCl_2]^+$ (**7b**), the ellipticilty profile is rather similar to **8**, albeit asymmetric along the C_α–C_β bond and less pronounced than for **8**. For the eclipsed conformer **7a**, the

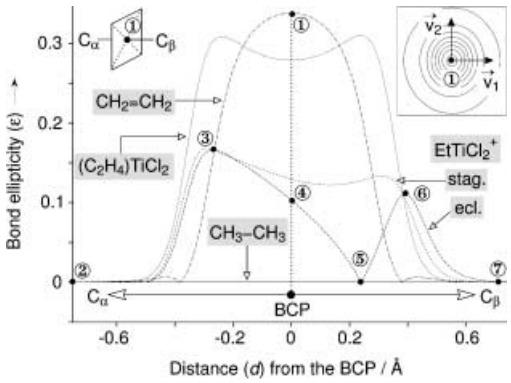

Figure 4. Calculated bond ellipticity profiles along the C_α–C_β bond path of $[EtTiCl_2]^+$ (**7a**: eclipsed; **7b**: staggered) in comparison with C_2H_6, C_2H_4, and $[(\eta^2\text{-}C_2H_4)TiCl_2]$ (**8**). The definition of the bond ellipticity is illustrated by the $\rho(\boldsymbol{r})$ contour map in the upper right corner, showing the charge density in the plane perpendicular to the bond path at the C–C bond CP of C_2H_4 (denoted "1" in this figure). ε is thus a measure of the cylindricity of the charge distribution $\rho(\boldsymbol{r})$: $\varepsilon = \lambda_1/\lambda_2 - 1$ (with $\lambda_1 < \lambda_2 < 0$). λ_i are eigenvalues of the corresponding eigenvectors $\boldsymbol{v}_1$ and $\boldsymbol{v}_2$ of the Hessian matrix of $\rho(\boldsymbol{r})$.

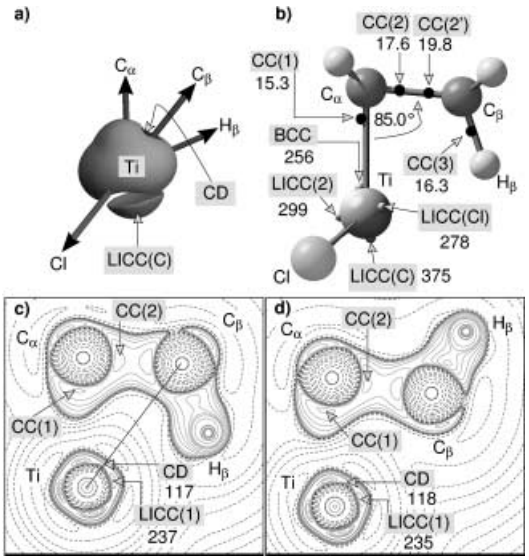

Figure 5. a) Envelope map of the negative Laplacian ($L(\boldsymbol{r}) = 150$ e Å^{-5}) for the Ti center in $[EtTiCl_2]^+$ (**7a**). b) DFT model of **7a** showing the relative location of the critical points in the $L(\boldsymbol{r})$ function. c), d) Contour plots of $L(\boldsymbol{r})$, in the Ti-C_α-C_β-H_β plane of **7a** and **7b**, respectively. Default contour levels (extra line at 200 eÅ^{-5}) as defined in Figure 1 were used.

π-system is even more distorted on the evidence of its ellipticity profile.[46] Here $\varepsilon_{max} = 0.17$, and is located close to the α-carbon atom. At a first glance, the π-character of the C_α–C_β bond appears more pronounced in the vicinity of C_α. At the bond CP a much lower value ($\varepsilon = 0.10$, denoted "4" in Figure 4) is found, and a second maximum is evident close to C_β ($\varepsilon_{max} = 0.11$).

This second, smaller maximum might arise from electronic distortion of the formally sp^3-hybridized β-carbon atom on account of the hypervalent character induced by the additional Ti···C_β interaction.[7a] We note that already at this stage, the polarization of an agostic β-carbon atom can be clearly revealed by the $L(\boldsymbol{r})$ function. Thus, the $L(\boldsymbol{r})$ contour map of **7b** (Figure 5d) shows the agostic C_β atom to display a charge concentration directed toward the metal center, whereas a typical non-agostic C_β atom displays a region of charge depletion facing the metal center (see for example Figure 10d). The first maximum, however, clearly arises from the significant electronic distortion at the α-carbon atom caused by the close-to-merging situation in the Ti-C_α-C_β plane of the two carbanionic CC(1) and the C-C-directed CC(2) features at C_α (Figure 5c, d). In fact, the ellipticity profile of **7a** (Figure 4), reveals ε_{max} to lie close to C_α, corresponding to a degree of retained carbanion character at the α-carbon atom, albeit significantly less than in $[C_2H_5]^-$ and EtLi (**4**).[7f] A similar ellipticity profile as in **7a** was found experimentally for the C_α–Si bond in $[2\text{-}(Me_3Si)_2CLiC_5H_4N]_2$ (**3**).[7e,f] In this case the carbanion character of C_α is clearly reduced by negative hyperconjugation and through additional electrostatic Li···C_γ and Li···H_γ interactions.[7e,f] Hence, negative hyperconjugation also seems to play an important role in the delocalization of the M–C bonding electrons observed in agostic complexes of early transition metals, even though weak but nonetheless significant secondary M···H interactions are evident in such cases.[7c,d]

We conclude that the ellipticity profiles characterizing C_α–X_β bonds (X = C, Si) may be used in a general manner to reveal electronic distortion of the α-C or β-X atom caused by delocalization of M–C bonding electron density into the C_α–X_β bonding region. It is worth noting at this point that ellipticity profiles for β-agostic ethyl groups of late transition metal alkyls resemble closely those of alkene complexes, indicating a much greater degree of M–C electron delocalization; and according with the classical picture that these systems are close to β-hydride elimination, possessing a high degree of C=C and M–H bond character.[47–49]

The bond ellipticity profiles of agostic lithium organyls or early transition metal alkyl complexes, which may be based on either experimental or theoretical charge densities, thus account in a unique and reproducible manner for electron delocalization arising mainly from negative hyperconjugation. The sensitivity of this new criterion of delocalization is strikingly illustrated by comparing the profiles of the staggered and eclipsed conformers of $[EtTiCl_2]^+$ (**7**). As noted above, the profile for the staggered conformer **7b** closely resembles that of the metallacycle **8**. This is remarkable, since the two conformers of **7** cannot be clearly distinguished on the basis of their relative energies.[7c, 44] Furthermore, the MOs which contribute to the agostic interaction show no significant differences in their density contours between **7a** and **7b** (Figure 6). Even the $L(\boldsymbol{r})$ functions reveal no measurable differences in the polarization of the metal atom (Figure 5c and d). Only the bond ellipticity profiles are sufficiently sensitive to reveal the subtly different nature of the ethyl ligand in the two conformers of **7**.

The nature of agostic interactions in d^0 metal complexes: In the previous Section on the charge concentration in $[EtCa]^+$, we showed that the proximal C_β–H_β fragment in $[EtCa]^+$ (**2**) causes a depletion in the magnitude of *cis*-LICC(1). However, the magnitude of *cis*-LICC(1) is in general rather independent

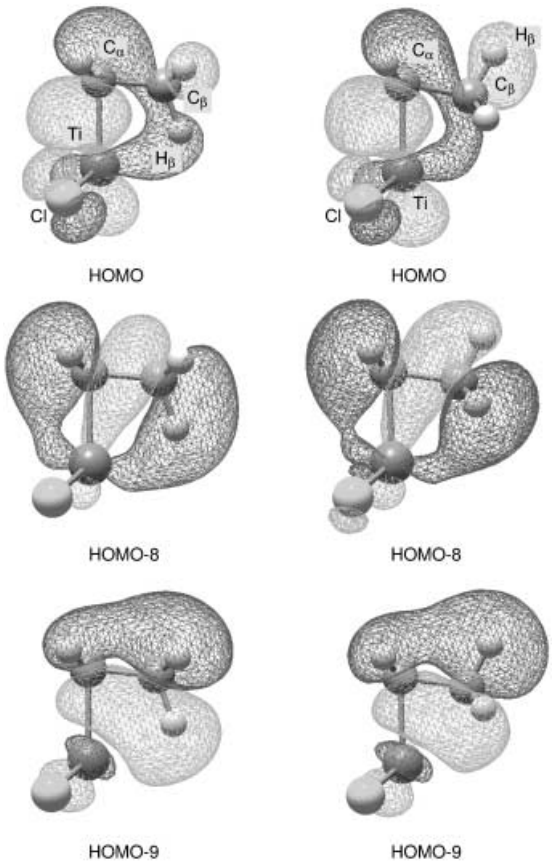

Figure 6. Constant probability density surfaces for the salient orbitals contributing to the interaction between Ti and the ethyl group of $[EtTiCl_2]^+$ (**7a**) and (**7b**), respectively.

of the orientation of the agostic C_β–H_β fragment, being virtually identical in **7a** and **7b** (237 and 235 e Å^{-5}, respectively). This agrees with a wide range of experimental and theoretical studies we have carried out on a variety of d^0 metal systems, which have shown that the M···H component of agostic interactions in complexes of lithium,[7e,f] early transition metals,[7a–d] or bimetallic lanthanide aluminates[50] makes only a modest contribution to the total agostic bonding. The similarities in the $L(\boldsymbol{r})$ plots for $[(\eta^2\text{-}C_2H_4)TiCl_2]$ (**8**) and both conformers of **7**, Figure 8c and Figure 5c, d, respectively, suggest an alternative driving force for β-agostic interactions in early transition metal alkyl complexes. In **7** the agostic interaction appears to be established primarily between the metal and the β-carbon atom (Ti···C_β). In comparison, in the metallacycle **8**, this Ti···C interaction has strengthened, and a pronounced covalent interaction now exists between Ti and C_β. Thus, the CC denoted LICC(1) in **7** has evolved in **8** into a well defined bonding CC denoted BCC (Figure 5c, d and Figure 8c). Interestingly, the relative positions at the metal center of LICC(1) and BCC in **7** and **8**, respectively, remain unaltered.[51] We note also that the bonding in both conformers of $[EtTiCl_2]^+$ (**7**) is related to that in the isoelectronic coordination complex $[(\eta^2\text{-}CH_2NH_2)TiCl_2]^+$ (**9**), in which the terminal methyl group of **7** has been replaced by a NH_2 donor group (Figure 8d). The $L(\boldsymbol{r})$ contour maps for **8** and **9**, shown in Figure 8c and f, represent the two extreme cases of covalent and donor interactions between the metal center and the terminal alkyl group CH_2X ($X = CH_2^-$, NH_2, for **8** and **9**, respectively), with the agostic system **7** ($X = CH_3$) representing an intermediate situation.

This is elegantly illustrated by the $L(\boldsymbol{r})$ contour maps of **7a**, (Figure 7a–c), which are oriented perpendicular to the C_s symmetry plane and include the Ti–C_α, the Ti–C_β and the Ti–H_β vector, respectively. The plot along the Ti–C_α vector displays a pattern typical of a polar covalent bond, with a pair of facing CCs for the two bonding partners (denoted CC(1) and BCC). The situation is radically different along the Ti–C_β directrix: here a CC (3, −1 CP) at the C_β atom faces a region of charge depletion (CD) [(3,+1) CP] at the metal atom, similar to the Ti···N donor–acceptor interaction in **9**. The same is true for the agostic β-hydrogen atom: The $L(\boldsymbol{r})$ contours indicate a charge polarization toward a region of locally increased Lewis acidity at the metal center ($L(\boldsymbol{r}) = 224$ e A^{-5}),[52] albeit less pronounced than the one facing the β-C atom ($L(\boldsymbol{r}) = 117$ e A^{-5}) (Figure 7b, c). Thus, the Ti···H component seems to be less important than the Ti···C_β interaction.

So what is the role of the agostic hydrogen atom in β-agostic systems of early transition metal complexes? As outlined above, and in accord with earlier investigations, it appears to make only a modest contribution to the total β-agostic bonding interaction. This situation is perhaps best illustrated by $[EtCa]^+$ (**2**), which is distorted from genuine C_s molecular symmetry [τ(Ti-C-C-H) = 15.2°]. In the case of $[EtTiCl_2]^+$ (**7a**), the agostic H_β atom is trapped in the cleft between the two CCs opposing the Cl atoms (Figure 7c). However, when

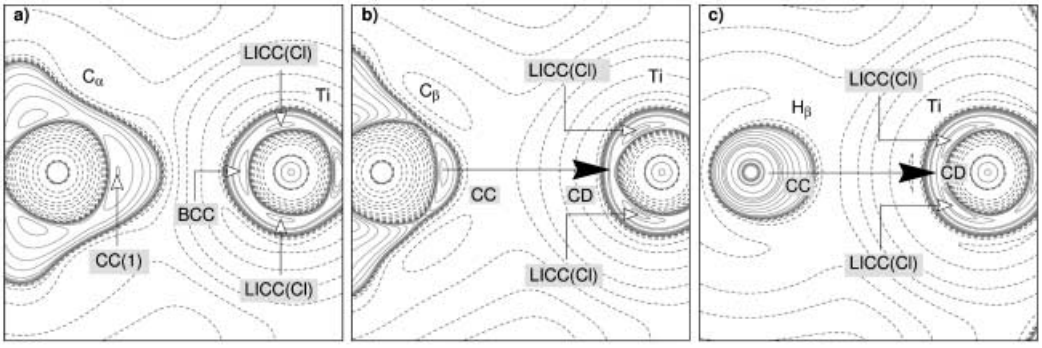

Figure 7. Contour plot of $L(\boldsymbol{r})$ in the plane perpendicular to the molecular C_s plane in $[EtTiCl_2]^+$ (**7a**), which includes a) the Ti and C_α atoms; b) the Ti and C_β atoms; and c) the Ti and H_β atoms. Default contour lines (additional contour line at 200 eÅ^{-5}).

the symmetry is lowered to C_1 by replacing one α-hydrogen atom by a methyl group (model **7c**), the agostic H_β atom in **7c** is displaced out of the Ti-C_α-C_β plane [τ(Ti-C-C-H) = −16.8°] as in $[EtCa]^+$ (**2**). Simultaneously, the Ti···H_β distance is increased compared with **7a** (2.035 and 2.067 Å for **7a** and **7c**, respectively), in accord with previous observations. In fact, all β-agostic alkyl complexes characterized to date appear to display wide C_α-C_β-H_β angles (>113°),[7a–d, 50] showing the β-H atoms to be bent *away* from the metal center. Experimental and theoretical charge density studies of $[EtTiCl_3(dmpe)]$ (**5**) and $[EtTiCl_2]^+$ (**7**)[7c, 42] have revealed in each case significant exocyclic curvature of the Ti–C_α bond path. Hence, it appears that the β-agostic H atom in **7a** and the two out-of-plane H atoms at the β-carbon atom in **7b** may actually *hinder* a close Ti···C_β approach and a more covalent Ti···C_β interaction.

Metal polarization and the extent of delocalization: In this Section we consider how the extent of electron delocalization in d^0 metal alkyl complexes is dictated by the polarization of the metal, and we present a concept for introducing and manipulating sites of local Lewis acidity at a metal center.

We start with an analysis of the electronic structures of a series of complexes $[EtTiCl_2 \cdot L]^+$ [where L = i) a strong π-acceptor (CO or PF_3), ii) a weak π-acceptor (PMe_3), iii) a σ-donor (H^-, CH_3^- or NMe_3), or iv) a π-donor ligand (Cl^-, F^- or OMe_2)]. Figure 9 outlines the main differences in the coordination modes of the various ligands. All π-acceptors display acute C-Ti-L and BCC-Ti-*cis*-LICC(2) angles. Thus, π-acceptor ligands directly face *cis*-LICC(2), which corresponds to a site of locally reduced Lewis acidity. This site is avoided by all σ-donor or π-donor ligands, which prefer instead to coordinate between *cis*-LICC(2) and *trans*-LICC—a site of locally enhanced Lewis acidity at Ti. These differences are in accord with general chemical considerations such as the HSAB principle.[53]

The π-acceptor ligands cause the Cl-Ti-Cl angle to widen relative to **7a** (∢ClTiCl 118.4°) when they coordinate to Ti, resulting in a shift of the corresponding *trans*-LICC(Cl) further out of the molecular plane (Figure 9).[54] In addition, the magnitude of the CC at the opposed coordination site decreases with increasing π-character of L, thereby assisting the β-agostic interaction: for L = PMe_3 (**10a**), PF_3 (**10b**), and CO (**10c**) *cis*-LICC(1) has values of 309, 282, and 299 e A^{-5}, with corresponding acute Ti-C-C angles of 85.5, 82.8, and 82.9°, respectively in $[EtTiCl_2 \cdot L]^+$.[55] In contrast, the σ- and π-donor ligands induce an axial polarization of the metal, with the donor electron pair causing a depletion of charge on the near side of the metal and an increased CC opposed to the Ti–L bond, resulting in a shift of LICC(1) toward BCC.[56] The angle between BCC and *cis*-LICC(1) decreases to well below

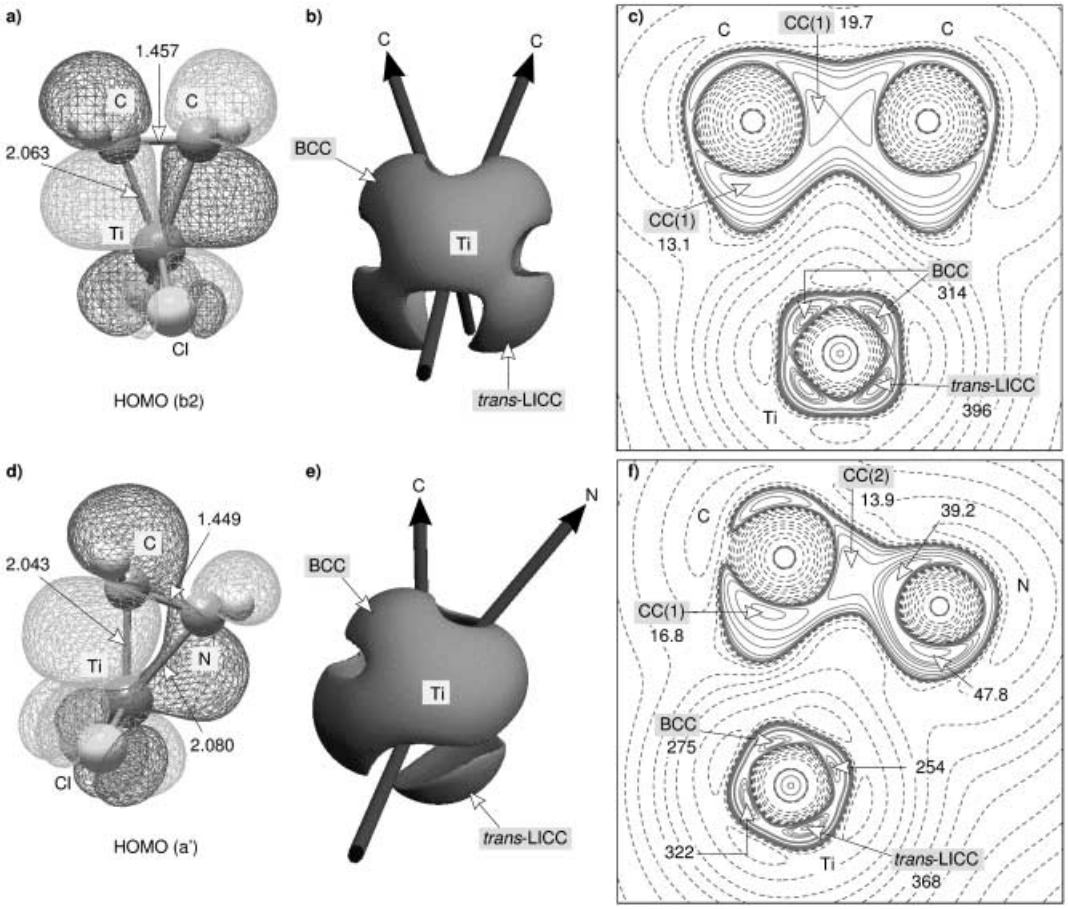

Figure 8. a), d) Constant probability density surfaces of the HOMO of $[(\eta^2\text{-}C_2H_4)TiCl_2]$ (**8**) and $[(\eta^2\text{-}(CH_2NH_2)TiCl_2]^+$ (**9**), respectively. b), e) Envelope maps of the negative Laplacian [$L(\boldsymbol{r}) = 160$ e $Å^{-5}$] for the titanium center in **8** and **9**, respectively. c), f) Contour plots of the negative Laplacian of the charge density, $L(\boldsymbol{r})$, in the Ti-C-X plane (X = C, N) of **8** and **9**, respectively. Default contour levels (additional contour line at 200 e$Å^{-5}$) as defined in Figure 1 were used.

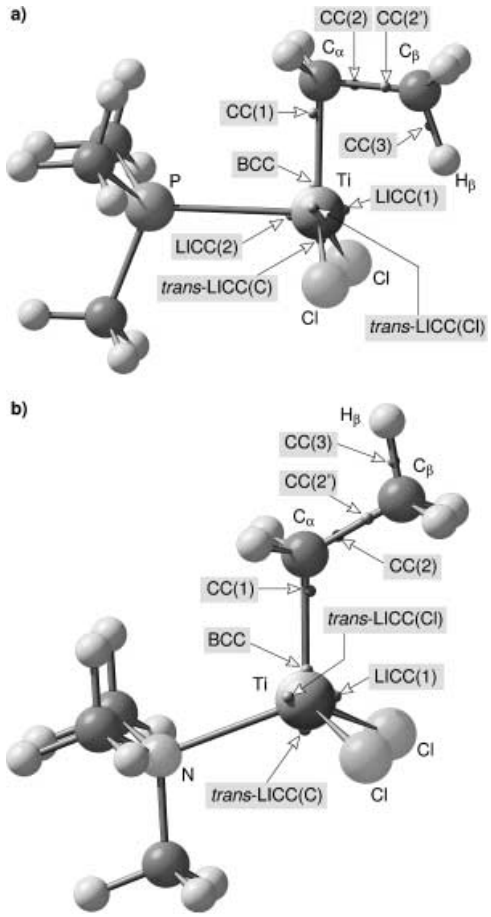

Figure 9. DFT models for a) $[EtTiCl_2 \cdot PMe_3]^+$ (**10a**) and b) $[EtTiCl_2 \cdot NMe_3]^+$ (**11a**) showing the location of salient CPs in $L(\boldsymbol{r})$. Important distances [Å] and angles [°] for **10a** and **11a**, respectively: Ti–C 2.031 (2.013), C_α–C_β 1.526 (1.528), C_β–H_β' 1.130 (1.095), Ti···H_β' 2.092 (Ti···H_β'' 3.307), ∢TiCC 85.5 (119.9), ∢CCH′ 114.7 (109.8), ∢CTiP(N) 89.1 (110.9), ∢ClTiCl 127.1 (115.6), ∢LICC(2)-Ti-BCC 88.0, ∢LICC(1)-Ti-BCC 90.9 (79.6). Atoms in or out of the symmetry plane are denoted by (′) and (″), respectively.

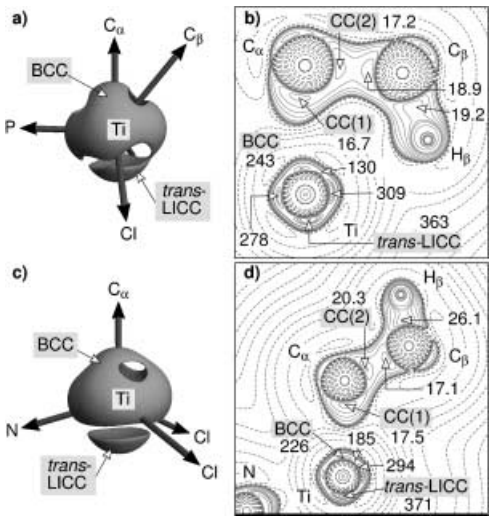

Figure 10. a), c): Envelope maps of the negative Laplacian [$L(\boldsymbol{r}) = 160\ e\,Å^{-5}$] for the Ti center in $[EtTiCl_2 \cdot PMe_3]^+$ (**10a**) and $[EtTiCl_2 \cdot NMe_3]^+$ (**11a**). The pronounced CD facing C_β in **10a** is reduced in **11a** due to the presence of the σ-donor ligand. b), d) Contour plots of the negative Laplacian of the charge density, $L(\boldsymbol{r})$, in the Ti-C_α-C_β-H_β plane for **10a** and **11a**, respectively. Default contour levels (additional contour line at 200 $e\,Å^{-5}$) are as defined in Figure 1.

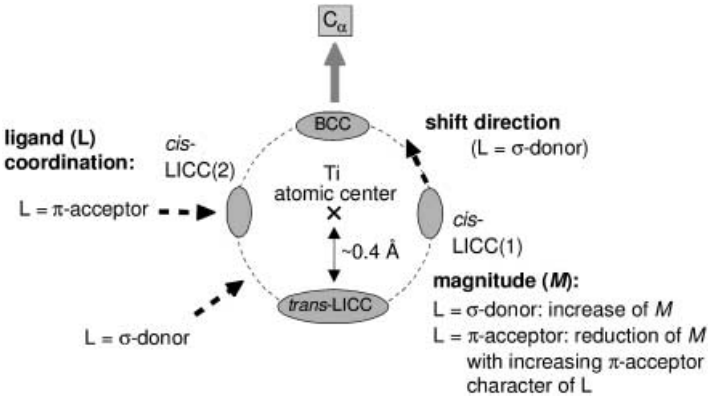

Figure 11. Ligand-induced polarization pattern of the Ti atom in $[EtTiCl_2 \cdot L]^+$ complexes **10a** (L = PMe_3), **10b** (L = PF_3), **11a** (L = NMe_3), **11b** (L = OMe_2) and **11c** (L = OMe_2; with ∢CTiO fixed at 180°).

90° (82.0° for L = NMe_3 (**11a**) or OMe_2 (**11b**); 80.1°), and the pronounced site of local Lewis acidity facing C_β in $[EtTiCl_2]^+$ (denoted "CD" in Figures 5c and 7b) is correspondingly reduced: 117, 185, and 183 $e\,A^{-5}$ in **7a**, **11a**, and **11b**, respectively.[57] As a consequence, the agostic interaction is no longer favored in any of these complexes, which display normal Ti-C-C angles of 119.9, and 117.6° for **11a** and **11b** (Figures 10 and 11).

Thus, π-acceptor ligands *trans* to the agostic β-CH fragment in our benchmark system **7a** support a β-agostic interaction, whereas σ- or π-donor ligands in the same position disfavor the interaction.[58] In contrast to the original suggestion by Brookhart and Green,[6] it is not the global Lewis acidity of the metal center, but the locally induced sites of increased Lewis acidity and the flexibility of the M–C_α bond which determine the extent of agostic interactions. This is perhaps best illustrated by our model system $[EtTiCl_2 \cdot OMe_2]^+$ (**11c**), which shows a fixed ∢C_α-Ti-O of 180°. Here, the O-donor ligand faces the ligand induced CC (*trans*-LICC) of the ethyl ligand. This configuration results in a weakening of the Ti–C bond relative to **11b** (Ti–C 2.079 vs 2.016 Å, respectively), and also gives rise to an enforced Lewis acidic site at the metal atom (CD = 130 and 183 $e\,Å^{-5}$, for **11c** and **11b**, respectively), which opposes the β-CH fragment.[59] Thus, in **11c** a pronounced agostic ethyl conformation (∢TiCC 82.9°, Ti···H_β 1.977 Å) results, despite the presence of a σ-donor ligand. This again demonstrates that agostic interactions are controlled by local ligand effects which dictate the polarization of the metal center. An in-depth analysis of the nature of individual metal–ligand interactions, and of the interplay between these at the metal center, has thus allowed us to attain a fuller understanding of the factors involved in β-agostic bonding, leading to enhanced predictive power and more reliable conclusions.

Conclusions

We have examined a range of d^0 metal ethyl complexes and related systems by a combination of experimental and theoretical techniques. In spite of previous controversy over the nature and origin of bonding and nonbonding CCs in the outer shell of the core of transition metal atoms,[26] we have shown these to be clearly revealed in the Laplacian of the experimental charge density for [$EtTiCl_3$(dmpe)] (**5**). Calculations on $[EtCa]^+$ (**2**), which possesses but a single ligand, have demonstrated that these CCs arise from involvement of $(n-1)$d metal orbitals in the M–L bond; and we have identified both *cis*- and *trans*-LICCs as a consequence. *trans*-LICCs or LOCCs have previously been proposed to be responsible for the non-VSEPR geometries displayed by many d^0 metal complexes,[15] but *cis*-LICCs have not been reported previously.

The magnitude of the CCs at the α- and β-carbon atoms of an ethyl ligand can be used to chart the extent of delocalization of the M–C bond.[7f] The *cis*-LICCs and the CD facing the β-methyl group in a d^0 metal ethyl complex play a critical role in hindering or encouraging the development of a β-agostic interaction in a manner fully in accord with the molecular orbital model of the interaction,[7a] which considers the stabilization to derive from delocalization of the M–C bonding orbital with the concomitant close M···H contact being a consequence rather than the cause of the interaction.[60]

Bond ellipticity (ε) profiles have been calculated for the C_α–C_β bond of $[EtTiCl_2]^+$ (**7**), and compared with those of related molecules. The asymmetry in ε corresponds to the degree of π character in the C–C bond, whereas the position and magnitude of ε_{max} reveals the extent to which the M–C bond is delocalized.

Analysis of CCs and of bond ellipticities provides a novel and general method for quantifying the extent of electron delocalization. These criteria benefit from the advantage of being derived from the charge density of a molecular system, and are thus physical observables that may be accessed both through experiment and by calculation. Hence, these simple criteria offer new direct experimental measures of electron delocalization, and open up exciting possibilities for the exploration of this phenomenon in a wide range of chemical situations.

An understanding of the way in which the ancillary ligands induce polarization at the metal center, and of the interplay between these effects and the metal–alkyl bonding, affords the possibility to predict—and hence to control and direct—the development of an agostic interaction with an alkyl ligand in a particular situation. Such predictive power is unprecedented in this area of chemistry. Detailed analysis of molecular charge distribution thus holds out the prospect of significant advances in the design and chemical control of complexes with central relevance to many reactions of academic and commercial importance.

Experimental Section

X-ray diffraction study of [$EtTiCl_3$(dmpe)] (5): A high purity crystalline sample of **5** was prepared as described in ref. [7a]. For the charge density study we combined two X-ray experiments using a CCD and an imaging plate detector system, both being connected to the same rotating anode assembly. In the following all data of the latter experiment are given in square brackets.

Data collection: A red, rhombic crystal with the dimensions $0.50 \times 0.25 \times 0.10$ mm [$0.20 \times 0.10 \times 0.05$ mm] was glued inside a 0.01 mm thin-walled capillary and mounted on a Kappa-CCD system from Nonius [imaging plate system from Stoe (IPDS)]. The sample was cooled with an Oxford Cryostream System to 105 K in 3 h with a mean temperature gradient of -1 K min^{-1}. Preliminary examination and final data collection were carried out with graphite-monochromated MoK_α radiation ($\lambda = 0.71073$ Å) generated from a Nonius FR 591 rotating anode running at 50 kV and 80 mA. Intensity data were collected using 1° φ- and ω scans [1° φ scans] with a detector-to-sample distance of 40 mm [75 mm]. For the low order data a scan set with 360 frames was collected at a scan angle (Θ) of 17.662° and a scan time of 70 s per frame. For the high order data two scan sets (213 frames in total; $\Theta = 30.928°$ and $\Theta = 31.480°$) with a scan time of 200 s per frame were chosen.[61a] [For the second crystal 360 frames at $\Theta = 0°$ with 300 s/frame were collected].

Data reduction: Crystal data for [$EtTiCl_3$(dmpe)] at 105 K: $C_8H_{21}Cl_3P_2Ti$, $M_r = 333.43$, $a = 7.8295(2)$, $b = 16.1104(2)$, $c = 11.8216(3)$ Å, $\beta = 91.6130(13)°$, $V = 1490.54(6)$ Å^3; monoclinic; space group $P2_1/n$; $Z = 4$; $F(000) = 688$; $\rho_{calcd} = 1.495$ g cm^{-3}; $\mu = 1.30$ mm^{-1}. The unit cell was determined from 87498 reflection positions. An initial orientation matrix was determined from 10 frames of the first scan set and refined during the integration of the scan sets of the first crystal. The intensities were first corrected for beam inhomogeneity and crystal decay by the program "Scalepack" ["Decay"] using a tight scale restraint (0.0001).[61b]

An absorption correction was then applied ($T_{min} = 0.61$; $T_{max} = 0.65$) [$T_{min} = 0.81$; $T_{max} = 0.85$] and symmetry equivalent and multiply measured reflections were averaged with the program "Sortav".[62] The internal agreement factor was $R_{int}(I) = 0.029$ [0.025] for a total of 35928 [16334] reflections yielding 13425 [3205] unique reflections. Both data sets together provided 99.8% of data in $5.8 < 2\Theta < 102.5°$ ($\sin\Theta/\lambda < 1.097$ Å^{-1}).

Multipolar refinements and determination of the deformation density: First, an independent atom model (IAM) refinement was carried out, in which all atoms were treated as spherical. Anisotropic thermal parameters were introduced to describe the thermal motion of all non-hydrogen atoms. All hydrogen atoms were found in the difference map and refined isotropically. The refinement finally converged at $R_1 = 0.040$, $wR_2 = 0.087$ and GOF = 1.039 for 11988 reflections ($\sin\Theta/\lambda < 1.05$ Å^{-1}), 211 parameters and maximum and minimum values of the residual density of 0.89 and -1.11 e Å^{-3}, respectively.[63]

A multipole model was then adopted to describe the deformation of $\rho(\boldsymbol{r})$ from a spherical distribution. According to a method proposed by Stewart,[64] the electron density $\rho(\boldsymbol{r})$ in a crystal is described by a sum of aspherical pseudoatoms at the nuclear positions $\{\boldsymbol{R}_j\}$:

$$\rho(\boldsymbol{r}) = \sum_j \rho_j(\boldsymbol{r} - \boldsymbol{R}_j)$$

Based on the Hansen–Coppens formalism,[65] the pseudoatom density $\rho_j(\boldsymbol{r} - \boldsymbol{R}_j)$ is expressed in terms of multipoles:[66]

$$\rho_j(\boldsymbol{r}_j) = P_c\rho_c(r_j) + \kappa'^3 P_v\rho_v(\kappa' r_j) + \sum_{l=0}^{l_{max}} \sum_{m=-l_{max}}^{+l_{max}} \kappa''^3 P_{lm} R_l(\kappa'' r_j) Y_{lm}(\theta_j, \varphi_j)$$

In the refinement of our best model the multipole expansion was truncated at the octapole level ($l_{max} = 3$) for carbon, phosphorus and chlorine and at the hexadecapole level for titanium. The hydrogen atoms were treated with monopoles ($l = 0$) and bond-directed dipoles ($l = 1$), in addition. Core and spherical valence densities were constructed using Clementi and Roetti Hartree-Fock (HF)[67a] atomic wave functions expanded over Slater-type basis functions. The radial functions for the valence deformation densities were of single Slater-type.[67b]

During the refinement the hydrogen atom positions were fixed at the values obtained by calculation. To reduce the number of multipole populations to be refined all methyl group carbons of the dmpe ligand [C(3), C(4), C(7) and C(8)], the methylene carbons C(5) and C(6), the axial chlorines Cl(2) and Cl(3), all methyl group hydrogens of the DMPE ligand

and the hydrogens H(11), H(12) and H(21), H(23), respectively, were assumed to be chemically equivalent (chemically constrained model, see also S8–11). In addition, local C_3 pseudo-symmetry was imposed on C(3), C(4), C(7) and C(8), and a local pseudo-mirror plane on Ti, C(1), C(2) and Cl(1). A radial scaling (κ') for the spherical density was refined for each heavy atom type while for hydrogen atoms κ' was kept fixed (1.20). In addition, for chemically non-equivalent atoms different κ' factors were used (14 in total). The molecule was kept neutral during all refinements. With the experimental model this procedure refined to $\kappa' = 1.312(16)$ for Ti, $\kappa' = 0.970(2)$ for Cl(1), $\kappa' = 0.9678(16)$ for Cl(2) and Cl(3), $\kappa' = 0.961(5)$ and 0.952(4) for P(1) and P(2), respectively, $\kappa' = 0.966(6)$ for C(1), $\kappa' = 0.996(7)$ for C(2), $\kappa' = 0.945(3)$ for C(3), C(4), C(7) and C(8) and $\kappa' = 0.952(4)$ for C(5) and C(6). The final agreement factors were $R_1 = 0.0268$, $wR_2 = 0.0284$ and GOF = 2.4389 for 12719 reflections ($F_o > 3\sigma(F_o)$; $\sin\Theta/\lambda < 1.05\,\text{Å}^{-1}$) and 256 parameters ($N_{ref}/N_{var} = 49.7$). The residual electron density map was practically featureless with the maximum and minimum values of 0.46 and $-0.34\,\text{e Å}^{-3}$ ($\sin\Theta/\lambda < 0.8\,\text{Å}^{-1}$), respectively (see also S12, Supporting Information for details).

Hirshfeld's rigid bond test[68] was applied to the atomic displacement parameters obtained from the refinements. The difference between mean-square amplitudes for all heavy atom bonds is within the limit of 1.0×10^{-3} Å^2, proposed by Hirshfeld, except for the P–C bond P(1)–C(5) [1.2×10^{-3} Å^2].

CCDC-204887 contains the supplementary crystallographic data for this paper. These data can be obtained free of charge via www.ccdc.cam.ac.uk/conts/retrieving.html (or from the Cambridge Crystallographic Data Centre, 12 Union Road, Cambridge CB21EZ, UK; fax: (+44)1223-336-033; or e-mail: deposit@ccdc.cam.ac.uk).

Computational details: All refinements were carried out with the full-matrix least-squares program "XDLSM" of the "XD" suite of programs;[66] the quantity minimized was $\varepsilon = \Sigma w_1(|F_o| - k\cdot|F_c|)^2$, where k is a scale factor, based on 12719 reflections with $F_o > 3\sigma(F_o)$. Weights were taken as $w_1 = 1/\sigma^2(F_o)$. Convergence was assumed when a maximal shift/esd $< 10^{-11}$ was achieved. For the topological analysis, critical points of the electron density were searched via a Newton–Raphson algorithm implemented in "XD". Properties of $\rho(\mathbf{r})$ and $\nabla^2\rho(\mathbf{r})$ were calculated after transformation of the local axis system into a global system.

DFT calculations using the Becke3LYP density functional[69] were carried out with the "Gaussian98" program suite (release A.7).[70] For all model systems the 6-311G(d,p)[71] basis set combination as specified in Gaussian98 was used (denoted I in the text). For Ca and Ti[72] one additional f-polarization function was employed. All geometry optimizations [except **1** (C_{3v}), **2** (C_1), **8** (C_{2v}), and **11c** (C_1)] were performed imposing C_s symmetry. The optimized geometries were verified as minima on the potential energy surface by computing analytical frequencies. In the case of the C_s geometry of **11b** one spurious imaginary frequency of $\omega = i33.5$ cm^{-1} was found. However, the energy and geometry of the C_1 model do not differ significantly.

The topological analysis of the theoretical and experimental electron densities was carried out with the "AIMPAC" software package[73] and the XD-program system,[74] respectively.

Acknowledgement

This work was supported by the Deutsche Forschungsgemeinschaft, and the Fonds der Chemischen Industrie. We thank King's College London for provision of a studentship (to E.G.), and for other support. We are also grateful for generous support from Prof. W. A. Herrmann and the Alexander von Humboldt Foundation (through a Post doctoral fellowship to D.S.).

[1] R. J. Gillespie, R. S. Nyholm, *Q. Rev. Chem. Soc.* **1957**, *11*, 339–380.
[2] G. S. McGrady, A. J. Downs, *Coord. Chem. Rev.* **2000**, *197*, 95–124.
[3] a) A. Haaland, A. Hammel, K. Rypdal, H. V. Volden, *J. Am. Chem. Soc.* **1990**, *112*, 4547–4549; b) V. Pfennig, K. Seppelt, *Science* **1996**, *271*, 626–628; c) S. Kleinhenz, V. Pfennig, K. Seppelt, *Chem. Eur. J.* **1998**, *4*, 1687–1691; d) M. Kaupp, *Chem. Eur. J.* **1998**, *4*, 1678–1686; e) M. Kaupp, *Chem. Eur. J.* **1999**, *5*, 3631–3643; f) M. Kaupp, *Angew. Chem.* **2001**, *113*, 3642–3677; *Angew. Chem. Int. Ed.* **2001**, *40*, 3534–3565.
[4] a) V. Jonas, G. Frenking, M. T. Reetz, *J. Comput. Chem.* **1992**, *13*, 919–934; b) V. Jonas, C. Boehme, G. Frenking, *Inorg. Chem.* **1996**, *35*, 2097–2099; c) G. S. McGrady, A. J. Downs, D. C. McKean, A. Haaland, W. Scherer, H. P. Verne, H. V. Volden, *Inorg. Chem.* **1996**, *35*, 4713–4718.
[5] a) Z. Dawoodi, M. L. H. Green, V. S. B. Mtetwa, K. Prout, *J. Chem. Soc. Chem. Commun.* **1982**, 802–803; b) Z. Dawoodi, M. L. H. Green, V. S. B. Mtetwa, K. Prout, *J. Chem. Soc. Chem. Commun.* **1982**, 1410–1411; c) Z. Dawoodi, M. L. H. Green, V. S. B. Mtetwa, K. Prout, A. J. Schultz, J. M. Williams, T. F. Koetzle, *J. Chem. Soc. Dalton Trans.* **1986**, 1629–1637.
[6] a) M. Brookhart, M. L. H. Green, *J. Organomet. Chem.* **1983**, *250*, 395–408; b) M. Brookhart, M. L. H. Green, L. L. Wong, *Prog. Inorg. Chem.* **1988**, *36*, 1–124.
[7] a) A. Haaland, W. Scherer, K. Ruud, G. S. McGrady, A. J. Downs, O. Swang, *J. Am. Chem. Soc.* **1998**, *120*, 3762–3772; b) W. Scherer, T. Priermeier, A. Haaland, H. V. Volden, G. S. McGrady, A. J. Downs, R. Boese, D. Bläser, *Organometallics* **1998**, *17*, 4406–4412; c) W. Scherer, W. Hieringer, M. Spiegler, P. Sirsch, G. S. McGrady, A. J. Downs, A. Haaland, B. Pedersen, *Chem. Commun.* **1998**, 2471–2472; d) D. C. McKean, G. S. McGrady, A. J. Downs, W. Scherer, A. Haaland, *Phys. Chem. Chem. Phys.* **2001**, *3*, 2781–2794; e) W. Scherer, P. Sirsch, M. Grosche, M. Spiegler, M. Mason, M. G. Gardiner, *Chem. Commun.* **2001**, 2072–2073; f) W. Scherer, P. Sirsch, D. Shorokhov, G. S. McGrady, S. A. Mason, M. G. Gardiner, *Chem. Eur. J.* **2002**, *8*, 2324–2334.
[8] L. Pauling, *The Nature of the Chemical Bond*, Cornell University Press, Ithaca, **1939**.
[9] L. Pauling, G. W. Wheland, *J. Chem. Phys.* **1933**, *1*, 362–374.
[10] a) E. *Z.* Hückel, *Physik* **1931**, *70*, 204–280; b) E. Hückel, *Physik* **1931**, *72*, 310–337; c) E. Hückel, *Physik* **1932**, *76*, 628–648.
[11] R. F. W. Bader, *International series of monographs on chemistry*, *Vol. 22: Atoms in Molecules—A Quantum Theory*, Oxford University Press, Oxford, **1990**.
[12] a) R. F. W. Bader, T. S. Slee, D. Cremer, E. Kraka, *J. Am. Chem. Soc.* **1983**, *105*, 5061–5068; b) D. Cremer, E. Kraka, T. S. Slee, R. F. W. Bader, C. D. H. Lau, T. T. Nguyen-Dang, P. J. MacDougall, *J. Am. Chem. Soc.* **1983**, *105*, 5069–5075; c) M. Tafipolsky, W. Scherer, K. Öfele, G. Artus, B. Pedersen, W. A. Herrmann, G. S. McGrady, *J. Am. Chem. Soc.* **2002**, *124*, 5865–5880; d) we note that σ-strain is another source of bond ellipticity. However, in our model systems σ-strain plays a minor role, since no C–C bond paths display any significant bond curvature.
[13] S. T. Howard, J. P. Foreman, P. G. Edwards, *Inorg. Chem.* **1996**, *35*, 5805–5812.
[14] See, for example: C. Heinemann, T. Müller, Y. Apeloig, H. Schwarz, *J. Am. Chem. Soc.* **1996**, *118*, 2023–2038.
[15] I. Bytheway, R. J. Gillespie, T.-H. Tang, R. F. W. Bader, *Inorg. Chem.* **1995**, *34*, 2407–2414.
[16] V. Calder, D. E. Mann, K. S. Sheshadri, M. Allavena, D. White, *J. Chem. Phys.* **1969**, *51*, 2093–2099.
[17] a) M. Hargittai in *Stereochemical Applications of Gas Phase Electron Diffraction*, *Vol. B* (Eds.: I. Hargittai, M. Hargittai), VCH, New York, **1988**, p. 383; b) M. Hargittai, I. Hargittai in *NATO ASI Series C: Mathematical and Physical Sciences*, *Vol. 410: Structures and Conformations of Non-Rigid Molecules* (Eds.: J. Laane, M. Dakkouri, B. van der Veken, H. Oberhammer), Kluwer, Dordrecht, **1993**; c) M. Hargittai, *Coord. Chem. Rev.* **1988**, *91*, 35–88; d) M. Hargittai, *Chem. Rev.* **2000**, *100*, 2233–2301.
[18] a) L. Seijo, Z. Barandiaran, S Huzinaga, *J. Chem. Phys.* **1991**, *94*, 3762–3773; b) M. Kaupp, P. v. R. Schleyer, H. Stoll, H. Preuss, *J. Am. Chem. Soc.* **1991**, *113*, 6012–6020; c) M. Kaupp, P. v. R. Schleyer, *J. Am. Chem. Soc.* **1992**, *114*, 491–497.
[19] a) L. Wharton, R. A. Berg, W. Klemperer, *J. Chem. Phys.* **1963**, *39*, 2023–2031; b) A. Büchler, J. L. Stauffer, W. Klemperer, *J. Chem. Phys.* **1964**, *40*, 3471–3473; c) A. Büchler, J. L. Stauffer, W. Klemperer, *J. Am. Chem. Soc.* **1964**, *86*, 4544–4550; d) E. F. Hayes, *J. Phys. Chem.* **1966**, *70*, 3740–3742.
[20] L. V. Von Szentpály, P. Schwerdtfeger, *Chem. Phys. Lett.* **1990**, *170*, 555–560.

[21] a) R. F. W. Bader, R. J. Gillespie, P. J. MacDougall, *J. Am. Chem. Soc.* **1988**, *110*, 7329–7336; b) R. F. W. Bader, P. J. McDougall, C. D. H. Lau, *J. Am. Chem. Soc.* **1984**, *106*, 1594–1605.

[22] See, for example: a) P. M. Morse, G. S. Girolami, *J. Am. Chem. Soc.* **1989**, *121*, 4114–4115; b) C. Pulham, A. Haaland, A. Hammel, K. Rypdal, H. P. Verne, H. V. Volden, *Angew. Chem.* **1992**, *104*, 1534–1537; *Angew. Chem. Int. Ed. Engl.* **1992**, *31*, 1464–1467; c) A. Haaland, W. Scherer, H. V. Volden, H. P. Verne, O. Gropen, G. S. McGrady, A. J. Downs, G. Dierker, W. A. Herrmann, P. W. Roesky, M. Geisberger, *Organometallics* **2000**, *19*, 22–29.

[23] R. F. W. Bader, H. Essén, *J. Chem. Phys.* **1984**, *80*, 1943–1960.

[24] a) R. P. Sagar, A. C. T. Ku, V. Smith, A. M. Simas, *J. Chem. Phys.* **1988**, *88*, 4367–4374; b) Z. Shi, R. J. Boyd, *J. Chem. Phys.* **1988**, *88*, 4375–4377; c) M. Kohout, A. Savin, H. Preuss, *J. Chem. Phys.* **1991**, *95*, 1928–1942; d) W.-T. Chan, I. P. Hamilton, *J. Chem. Phys.* **1998**, *108*, 2473–2485.

[25] a) P. J. MacDougall, M. B. Hall, R. F. W. Bader, J. R. Cheesemann, *Can. J. Chem.* **1989**, *67*, 1842–1846; b) R. J. Gillespie, I. Bytheway, T.-H. Tang, R. F. W. Bader, *Inorg. Chem.* **1996**, *35*, 3954–3963.

[26] R. F. W. Bader, R. J. Gillespie, F. Martín, *Chem. Phys. Lett.* **1998**, *290*, 488–494.

[27] For a definition of the bond path or atomic interaction line which follows the ridge of the charge density between bonded atoms see ref. [11].

[28] R. J. Gillespie, P. L. A. Popelier, *Chemical Bonding and Molecular Geometry*, Oxford University Press, Oxford, **2001**.

[29] Cremer and Kraka pointed out that analysis of $L(\boldsymbol{r}_c)$ gives a rather sensitive measure of the charge-density accumulation, but is not always sufficient to distinguish between covalent and closed-shell interactions. The chemical bonding can be described sufficiently only when both the electron-density based criteria and energetic contributions are taken into account. They therefore proposed analysis of the electronic kinetic energy density $G(\boldsymbol{r})$ and the electronic potential energy density $V(\boldsymbol{r})$ at the bond critical point, since the magnitudes of both are related to the Laplacian by an equation derived by Bader (R. F. W. Bader, *J. Chem. Phys.* **1980**, *73*, 2871–2883) namely $2G(\boldsymbol{r})+V(\boldsymbol{r})=\frac{1}{4}\nabla^2\rho(\boldsymbol{r})$. For covalent bonds it has been shown that the local energy density $H(\boldsymbol{r}_c)=G(\boldsymbol{r}_c)+V(\boldsymbol{r}_c)$ is less than zero (D. Cremer, E. Kraka, *Angew. Chem.* **1984**, *96*, 612–614; *Angew. Chem. Int. Ed. Engl.* **1984**, *23*, 627–628); and that, in addition, the ratio $G(\boldsymbol{r}_c)/\rho(\boldsymbol{r}_c)$ should be less than unity (P. Macchi, D. M. Proserpio, A. Sironi, *J. Am. Chem. Soc.* **1998**, *120*, 13429–13435). The ratio $G(\boldsymbol{r}_c)/\rho(\boldsymbol{r}_c)=0.71/0.69$ for **1** and **2**, respectively, is less than 1.0 Hartree e^{-1}; and, in addition, the local energy density $H(\boldsymbol{r}_c)=-0.09/-0.11$ Hartree Å^{-3} is slightly negative suggesting covalent character. We note however, that this is at odds with the conclusion of Gillespie, who suggested an ionic bond in $CaMe_2$; see ref. [15].

[30] S. Berger, W. Bock, G. Frenking, V. Jonas, F. Müller, *J. Am. Chem. Soc.* **1995**, *117*, 3820–3829.

[31] a) According to the NLMO analysis: %s(Ca) = 59.8/38.0 %, %p(Ca) = 0.3/1.0 %, %d(Ca) = 39.9/61.0 %, %f(Ca) = 0.0 %; %s(Ca) – %f(Ca) give the hybridization at Ca for the Ca–C bond in **1** and **2**, respectively; b) A. E. Reed, R. B. Weinstock, F. Weinhold, *J. Chem. Phys.* **1985**, *83*, 735–746; c) A. E. Reed, L. A. Curtiss, F. Weinhold, *Chem. Rev.* **1988**, *88*, 899–926; d) Gaussian NBO Version 3.1.

[32] On account of the C_{3v} symmetry of **1** three (3, –3) CPs are obtained at $L(\boldsymbol{r})=102.2$ e Å^{-5}. However, these are poorly resolved in the envelope map and are better described as a single diffuse feature.

[33] The global minimum established on the potential energy surface (PES) has C_1 symmetry, and shows a Ca-C_α-C_β-H_β torsional angle $\tau=15.2°$. Together with the wide C_α-C_β-H_β angle of 114.5° the β-H atom appears to be pushed away from, rather than attracted toward, the metal center. The DFT-calculated force field at the same level of theory (B3LYP/I) for a model with C_s symmetry shows a single imaginary frequency ($\omega=i62.2$), implying that the C_s geometry is a first order transition state unstable with respect to methyl rotation. The imaginary frequency found for the C_s model could be confirmed by employing the Grid = UltraFine and SCF = VeryTight option in Gaussian98 ($\omega=i57.2$). However, the energy difference between the C_s and C_1 geometries is insignificant (< 0.1 kcal mol^{-1}).

[34] It is the presence of the β-agostic C–H fragment which induces the development and polarization of the *cis*-LICCs, rather than vice versa: optimization of **2** with the Ca-C_α-C_β angle constrained at 112° (model **2a**) results in formation of a diffuse NBCC at the Ca atom similar to that observed for **1** showing also near-perfect cylindrical symmetry ($L(\boldsymbol{r})$ data for **2a**: BCC = 87.4, NBCC = 105.3, LICC = 105.2 e Å^{-5}). The total energy of this restrained conformer has increased by 0.92 kcal mol^{-1} relative to the agostic conformer at the B3LYP/I level of theory. This energy difference might be related to the magnitude of the agostic interaction; see ref. [7a].

[35] This is at odds with the earlier model for agostic interactions based on a 3c–2e interaction between the C–H bond and the metal center; see ref. [6].

[36] Only the κ parameter which allows expansion ($\kappa<1$) or contraction ($\kappa>1$) of the valence shell, and the P_v parameter (valence shell population parameter) at Ti have been refined to account for charge transfer between the metal center and the ligands.

[37] More precisely, Coppens et al. (A. Holladay, P. Leung, P. Coppens, *Acta Crystallogr. Sect. A* **1983**, *39*, 377–387) showed that the occupation of a d_{z^2} orbital relates to the multipole parameters as follows: $P(d_{z^2})=0.2P_v+1.04P_{20}+1.40P_{40}$. Thus, P_{40} is the dominating density contribution for a d_{z^2} density contour. The population parameter [$P_{40}=0.246(16)$] indicates that about 0.25 "electrons" are shifted from the negative to the positive regions of the corresponding hexadecapole (d_{40} with $l=4, m=0$). Refinement of all multipoles at Ti (C_s symmetry restrains) leads to the following even multipole populations ($P_{20}=-0.047$, $P_{21+}=-0.085$, $P_{22+}=0.035$, $P_{40}=0.246$, $P_{41+}=-0.029$, $P_{42+}=0.034$, $P_{43+}=-0.093$, $P_{44+}=-0.027$) which stress the dominant contribution of P_{40} for the d_{z^2} density contour. For a detailed description of the multipole model employed in this work see Experimental Section.

[38] We note that the polarization pattern of the metal atom in our experimental model for **5** is even closer to the one in our theoretical model of $[EtTiCl_2]^+$ (**7**) (Figure 5). This result might be attributed to the more ionic nature of **5** in the experimental solid state structure in comparison with the theoretical gas-phase model. Indeed the Ti–Cl bond length of 2.4223(2) Å in the solid state structure is remarkably long and suggests a significantly weakened Ti–Cl bond, albeit still intact.

[39] Further experimental support for the existence of LICCs is provided by a study of Bz_3Ti-O-$TiBz_3$, where LICCs have been detected *trans* to the Ti–C and Ti–O bonds, with experimental ρ values of 9.86 [$L(\boldsymbol{r})=353$] and 8.93 e Å^{-3} [$L(\boldsymbol{r})=256$ e Å^{-5}], respectively, and in good agreement with the corresponding theoretical values of 10.2 and 9.6 e Å^{-3} [$L(\boldsymbol{r})=350$ and 282 e Å^{-5}, respectively; W. Scherer, D. Shorokhov, H. M. I. Pritchard, G. S. McGrady, unpublished results; see Supporting Information]. The difference between LICC(C) and LICC(O) in this instance is nearly 1.0 e Å^{-3}, the upper limit for residual electron densities required for publication of X-ray diffraction structures in *Acta Crystallogr*. Hence, differences in ρ values between LICCs of 0.5 e Å^{-3} or more should be clearly observable in charge density studies.

[40] A. C. Cooper, E. Clot, J. C. Huffman, W. E. Streib, F. Maseras, O. Eisenstein, K. G. Caulton, *J. Am. Chem. Soc.* **1999**, *121*, 97–106.

[41] See, for example: J. Jaffart, R. Mathieu, M. Etienne, J. E. McGrady, O. Eisenstein, F. Maseras, *Chem. Commun.* **1998**, 2011–2012.

[42] P. L. A. Popelier, G. Logothetis, *J. Organomet. Chem.* **1998**, *555*, 101–111.

[43] L. Fan, D. Harrison, L. Deng, T. K. Woo, D. Swerhone, T. Ziegler, *Can. J. Chem.* **1995**, *73*, 989–998.

[44] At our standard level (B3LYP/I), the staggered conformation (**7b**) appears to be a first order transition state with respect to methyl group rotation ($\omega=i164.5$). However, the energy difference between the conformers **7b** and **7a** ($\Delta E_{stag,ecl}=1.5$ kcal mol^{-1}) is rather small, and this situation can easily be reversed using other basis set combinations such as the DZVP basis; see N. Godbout, D. R. Salahub, J. Andzelm, E. Wimmer, *Can. J. Chem.* **1992**, *70*, 560–571. In the latter case the staggered conformer becomes energetically favored on the potential energy surface.

[45] The double maximum feature can be attributed to the presence of *four* CCs at each olefinic carbon atom in [(η^2-C_2H_4)$TiCl_2$]. In contrast, at strictly sp^2 hybridized carbon atoms (e.g. in C_2H_4) only three CCs can be located. The *fourth* CC in [(η^2-C_2H_4)$TiCl_2$] is relatively weak but well resolved, and points toward the metal atom. This causes the

double maximum in the ellipticity profile of $[(\eta^2\text{-}C_2H_4)TiCl_2]$. We note that the magnitude of the metal directed CCs at olefinic carbon atoms might be used to estimate the degree of sp^3 hybridization.

[46] The ε profile of **7a** even shows a pronounced minimum along the C_α–C_β bond path at $d = 0.24$ Å ($\varepsilon = 0$). Furthermore, at this minimum (point labeled "5" in Figure 4) the major axis of curvature, denoted $\boldsymbol{\nu}_2$ in Figure 4, reverses its orientation with respect to the molecular plane. Indeed, at the first maximum of the ε profile of **7a** (labeled "3" in Figure 4), the major axis lies within the C_s molecular plane (in-plane) while it is oriented perpendicular (out-of-plane) at the second maximum (point denoted "6"). The inversion of the major axis $\boldsymbol{\nu}_2$ can be explained by the different magnitudes of the CCs at the β-carbon atom directed toward the three C–H bonds. The in-plane CC pointing toward the agostic H_β atom is significantly depleted (16.3 e Å^{-5}) compared with the corresponding out-of-plane CCs directed towards the non-agostic H atoms (28.3 e Å^{-5}). As a result the major axis of curvature is aligned out-of-plane between the points "5" and "7".

[47] The unusual character of the C_α–C_β bond in $[EtTiCl_3(dmpe)]$ (**5**) was pointed out by Green et al.; see ref. [5]. The original X-ray structure determination found a C–C bond length of 1.467(15) Å, implying partial double bond character and leading to the proposal of a frozen transition state for β-elimination (ref. [5]). Subsequent reinvestigation at low temperature found a value of 1.5117(12) Å, with no evidence of significant shortening (ref. [7c]). In this work, the C_α–C_β bond length was confirmed (1.513(1) and 1.521 Å in experiment and theory, respectively).

[48] Statistical analysis of the C_α–C_β bond lengths in transition metal ethyl compounds based on 107 X-ray structures in the Cambridge Structural Database 5.10 (see ref. [7a], [49]) yields an average of 1.475 Å. We note that C–C bond lengths may be systematically shortened by incomplete allowance for librational motion in simple harmonic refinement of atomic displacement parameters. This stresses the need for high order reflection data at low temperatures, and models which account for the aspherical features of the electron density, in order to obtain accurate bond lengths from X-ray data.

[49] F. H. Allen, O. Kennard, R. Taylor, *Acc. Chem. Res.* **1983**, *16*, 146–153.

[50] G. M. Klimpel, R. Anwander, M. Tafipolsky, W. Scherer, *Organometallics* **2001**, *20*, 3983–3992.

[51] LICC(1) represents a (3, –1) CP [saddle point in $L(\boldsymbol{r})$] in the TiCC plane of **7a** and **7b** and not a genuine (3, –3) CP as in the case of **8**.

[52] This region is located very close to the (3, –1) CP ($L(\boldsymbol{r}) = 237$ e Å^{-5} denoted LICC(1) in Figure 5c) which connects the two ligand-induced CCs of both chlorine ligands (LICC(Cl); Figure 7).

[53] See, for example: R. G. Pearson, *Coord. Chem. Rev.* **1990**, *100*, 403–425.

[54] In the case of π-acceptor ligands (**10a–c**) *cis*-LICC(2) renders into a bonding charge concentration which was nonbonding in **7a**, whereas for σ-donor ligands in the complexes **11a**, **b** it represents a (3, –1) CP. Furthermore, *cis*-LICC(1) develops from a (3, –1) CP in **7a** into a genuine (3, –3) CP for both, σ-donor (**11a**, **b**) and π-acceptor (**10a–c**) ligands employed in our study.

[55] This feature is in accord with theoretical treatments of the (kinetic) *trans* effect, whereby the stability of the transition state is dictated by the σ-donor and π-acceptor properties of the ligands. The π-effects are not really pronounced in the Lewis-acidic models **10a–c** but still noticeable. See, for example: a) F. Basolo, R. G. Pearson, *Mechanisms of Inorganic Reactions*, Wiley, New York, **1968**; b) C. H. Langford, H. B.Gray, *Ligand Substitution Processes* (Ed.: W. A. Benjamin), New York, **1965**; c) Z. Lin, M. B. Hal, *Inorg. Chem.* **1991**, *30*, 646–651.

[56] Following the suggestion of Frenking et al. (G. Frenking, S. Fau, C. M. Marchand, H. Grützmacher, *J. Am. Chem. Soc.* **1997**, *119*, 6648–6655), the π-donor ability of the halogens given by the p(π) population at atom A in AX_3^+ (A = C, Si, Ge, Sn, Pb; X = F, Cl, Br or I) is significant and increases for all cations in the order F < Cl < Br < I. On the contrary, the magnitude and relevance of π-donor capabilities of halide ligands in the early transition metal systems $[RTiCl_2]^+$ and $RTiCl_3$ (R = Me or Et) appears to be less clear. The non-agostic geometry of $MeTiCl_3$ and $EtTiCl_3$ might be explained by the pronounced π-donor ability of the chlorine ligands and the classification of both these benchmark systems as 18 VE species. However, the examples Me_2TiCl_2, and Me_3TiCl, which clearly have VE counts of less than 18, still display non-agostic structures despite the replacement of the π-donor Cl^- by the σ-donor CH_3^- (See, for example: a) ref. [4c]; b) G. S. McGrady, A. J. Downs, N. C. Bednall, D. C. McKean, W. Thiel, V. Jonas, G. Frenking, W. Scherer, *J. Phys. Chem. A* **1997**, *101*, 1951–1968; c) S. Kleinhenz, K. Seppelt, *Chem. Eur. J.* **1999**, *5*, 3573–3580.) Hence, the distinction between pure σ-donor and σ-donor/π-donor ligands does not appear to be crucial to the manipulation of agostic interactions in early transition metal alkyl complexes: both types of ligand weaken the agostic interaction of a C-H group in *trans*-position.

[57] a) These conclusions are in accord with theoretical treatments of the static *trans* effect or *trans* influence, whereby the stability of the ground state is dictated mainly by the σ-donor and to a lesser extent by the π-acceptor properties of the ligands. See, for example: T. G. Appleton, H. C. Clark, L. E. Manzer, *Coord. Chem. Rev.* **1973**, *10*, 335–422. Thus, as a spin-off from this study, both the *trans* effect and the *trans* influence may be rationalized in terms of charge density-based criteria. b) In the parent system $[EtTiCl_2]^+$ **7a**, the corresponding CD appears to be independent of the ∢TiCC angle and the ethyl group conformation: CD = 117 e Å^{-5} for ∢TiCC = 85.0° (eclipsed ethyl group conformation) and 118 e Å^{-5} for ∢TiCC = 112.0° (staggered ethyl group conformation). Thus, agostic Ti···C_β and Ti···H_β contacts do not appear to compensate significantly opposing regions of charge depletions—as expected for weak interactions. This might be a general and characteristic feature of agostic interactions in early transition metal alkyl complexes.

[58] It is noteworthy that the different types of bonding displayed by π-acceptor and σ- and π-donor ligands is clearly pronounced in our $[EtTiCl_2 \cdot L]^+$ model systems, in spite of the fact that π-back donation is usually not expected for d^0 systems. For example, the d^0 complex Cp_2TiCl_2 does not form a stable CO complex, whereas Cp_2Ti as a d^2-system does. Hence, our study of the $[EtTiCl_2^+ \cdot L]$ goes beyond simple rules based on VE counting, and provides a basis to visualize and to quantify weak π-interactions between π-acceptors (e.g. PF_3, CO) and nonbonding CCs located at Lewis acidic metal cations (e.g. in $[EtTiCl_2]^+$).

[59] Furthermore, the BCC (234 vs 291 e Å^{-5}; directed toward C_α) is quite different in **11b** and **11c**, respectively. Thus, the σ-donor coordination in the position *trans* to the alkyl group leads to an increase in the BCC.

[60] However, in the case of later transition metal ethyl complexes, M···H–C bonding does appear to play a significant role. This is revealed by characteristic structural features such as significant shortening of the C-C and elongation of the C_β–H bonds, and by the proclivity of the complexes to undergo β-hydride elimination. In these cases M···H–C bonding may be viewed as an intramolecular form of σ-complexation. See, for example: R. H. Crabtree, *Angew. Chem.* **1993**, *105*, 828–845; *Angew. Chem. Int. Ed. Engl.* **1993**, *32*, 789–805.

[61] a) COLLECT Data Collection Software, Nonius B. V., Delft (The Netherlands), **1998**; b) Z. Otwinowski, W. Minor, *Processing of X-ray Diffraction Data Collected in Oscillation Mode*, *Volume 276: Macromolecular Crystallography*, *Part A* (Eds.: C. W. Carter, Jr., R. M. Sweet), Academic Press, San Diego, **1997**, pp. 307–326.

[62] R. H. Blessing, *Acta Crystallogr. Sect. A* **1995**, *51*, 33–38.

[63] G. M. Sheldrick, SHELXL-97, Program for Crystal Structure Refinement, University of Göttingen, Göttingen (Germany), **1997**.

[64] R. F. Stewart, *Acta Crystallogr. Sect. A* **1976**, *32*, 565–574.

[65] H. K. Hansen, P. Coppens, *Acta Crystallogr. Sect. A* **1978**, *34*, 909–921.

[66] T. Koritsanszky, S. T. Howard, Z. Su, P. R. Mallinson, T. Richter, N. K. Hansen, XD, Computer Program Package for Multipole Refinement and Analysis of Electron Densities from Diffraction Data, Free University of Berlin (Germany), **1997**.

[67] a) E. Clementi, C. Roetti, *At. Data Nucl. Data Tables* **1974**, *14*, 177–478; b) E. Clementi, D. L. Raimondi, *J. Chem. Phys.* **1963**, *38*, 2686–2689.

[68] F. Hirshfeld, *Acta Crystallogr. Sect. A* **1976**, *32*, 239–244.

[69] a) A. D. Becke, *J. Chem. Phys.* **1993**, *98*, 5648–5652; b) C. Lee, W. Yang, R. G. Parr, *Phys. Rev. B* **1988**, *37*, 785–789.

[70] M. J. Frisch, G. W. Trucks, H. B. Schlegel, G. E. Scuseria, M. A. Robb, J. R. Cheeseman, V. G. Zakrzewski, J. A. Montgomery, Jr., R. E. Stratman, J. C. Burant, S. Dapprich, J. M. Millam, A. D. Daniels, K. N. Kudin, M. C. Strain, O. Farkas, J. Tomasi, V. Barone, M. Cossi, R. Cammi, B. Mennucci, C. Pomelli, C. Adamo, S. Clifford, J. Ochterski,

G. A. Petersson, P. Y. Ayala, Q. Cui, K. Morokuma, D. K. Malick, A. D. Rabuck, K. Raghavachari, J. B. Foresman, J. Cioslowski, J. V. Ortiz, A. G. Baboul, B. B. Stefanov, G. Liu, A. Liashenko, P. Piskorz, I. Komaromi, R. Gomperts, R. L. Martin, D. J. Fox, T. Keith, M. A. Al-Laham, C. Y. Peng, A. Nanayakkara, C. Gonzalez, M. Challacombe, P. M. W. Gill, B. Johnson, W. Chen, M. W. Wong, J. L. Andres, C. Gonzalez, M. Head-Gordon, E. S. Replogle, J. A. Pople, GAUSSIAN 98, revision A.7, Gaussian, Inc., Pittsburgh, PA, **1998**.

[71] a) R. Krishnan, J. S. Binkley, R. Seeger, J. A. Pople, *J. Chem. Phys.* **1980**, *72*, 650–654; b) A. D. McLean, G. S. Chandler, *J. Chem. Phys.* **1980**, *72*, 5639–5648; c) A. J. H. Wachters, *J. Chem. Phys.* **1970**, *52*, 1033–1036.

[72] In the case of the titanium atom a slightly modified contraction scheme was used (see Supporting Information for details) and the basis set was complemented with an additional f-polarization function (A. W. Ehlers, M. Böhme, S. Dapprich, A. Gobbi, A. Höllwarth, V. Jonas, K. F. Köhler, R. Stegmann, A. Veldkamp, G. Frenking, *Chem. Phys. Lett.* **1993**, *208*, 111–114).

[73] a) F. W. Biegler-König, R. F. W. Bader, T. Tang, *J. Comput. Chem.* **1982**, *3*, 317–328; b) J. R. Cheeseman, T. A. Keith, R. F. W. Bader, AIMPAC program package, McMaster University, Ontario (Canada), **1994**.

[74] As reported earlier (see ref. [12c]) we have noted a software bug in the official XD-release which resulted in erroneous ζ-values for transition metal atoms in the XDPROP module. However, this bug had no significant influence on most of the topological values of the previous charge density model of **5**. However, the Ti···H bond CP which was found in the previous study could not be verified by the new model using a corrected version of the XDPROP module (P. Macchi, M. Tafipolsky, Modifications to the XD code, unpublished). In any case, this result is in accord with our previous model, showing the gradient path between the ring and the Ti···H bond CPs to be extremely flat, with the bond and ring CPs almost merging into a singularity in ρ, a phenomenon characteristic of bond fission.

Received: March 3, 2003
Revised: June 13, 2003 [F4909]

